

Numerical Study of Shock Wave-Boundary Layer Interaction in Cylinder-Flare Configuration



T. Nakano, G. Lehnasch, and E. Goncalves

Abstract This study aims at characterizing shock wave/boundary layer interactions in conical configurations. This preliminary work focuses on the ramp configuration and presents some main differences observed in the statistical turbulence structure upstream and through the interaction region between the conical and planar case.

1 Introduction

The configuration of shock wave/boundary layer interactions (SWBLI) has been widely studied in planar geometries to characterize the distortion of near-wall turbulence structure [1] and identify some possible physical mechanisms at the origin of its distinctive low-frequency unsteadiness [2]. However, our knowledge of its exact features in more complex geometries is still lacking. A direct numerical simulation (DNS) of a supersonic boundary layer spatially developing over a cylinder-flare configuration is here carried out and the results are compared to a reference planar case. The ratio of boundary layer thickness (measured just upstream of the interaction region) over the curvature radius of the convex wall is $\delta_0/R \simeq 0.1$, which is expected to be already sufficient to lead to non-negligible curvature effects on the near-wall turbulence structure. This work aims at giving a preliminary assessment of the influence of such a geometrical effect on statistical turbulent properties of both the upstream development of the supersonic boundary layer and the shock/separation system.

T. Nakano (✉) · G. Lehnasch · E. Goncalves
Institut Pprime, CNRS, ISAE-ENSMA, Université de Poitiers, Futuroscope Chasseneuil, France
e-mail: tamon.nakano@ensma.fr

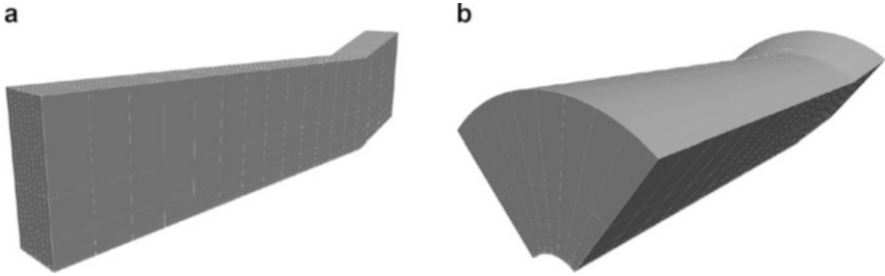


Fig. 1 Overview of computational domains. (a) Flat case. (b) Curved case

1.1 Numerical Method

The Navier-Stokes equations are discretized with high-order hybrid finite difference schemes in curvilinear coordinates. The convective flux is discretized by combining sixth-order optimized centered schemes (and selective filter) with fifth-order WENO schemes as a function of a shock sensor. The upstream Mach number of the airflow (assumed to be a perfect gas) is $M_0 = 3$, and the flow deflection imposed by the ramp geometry is 18° . These parameters are similar to the ones used by Adams [3]. Two types of computational domains and grids, illustrated in Fig. 1 for flat and curved case, are used to assess the influence of wall curvature in the azimuthal direction. Periodicity conditions are applied at the side boundaries in the azimuthal direction. The convex wall in the curved case follows a cylinder shape portion spanning 80.4° in the azimuthal direction. This azimuthal extent has been checked to be sufficiently higher than the integral turbulent length scales of the incoming boundary layer to avoid any artificial confinement effect. The upstream transition is triggered by adding sine wave perturbations of the inlet velocity profile, and the subsequent development of the supersonic turbulent boundary layer is simulated over the convex wall of the cylinder in an initially uniform region. The mesh has been refined to fulfill standard DNS requirements near the wall with mesh size reaching $\Delta_x^+ = 6.3$, $\Delta_r^+ = 0.6$, and $\Delta_\theta^+ = 4.1$ in the upstream developed turbulence region. The computational domain extends over lengths approximately equal to $L_x \simeq 154\delta_0^* \simeq 57\delta_0$, $L_r \simeq 12\delta_0 \simeq 33\delta_0^*$, and $L_\theta \simeq 5\delta_0 \simeq 13.5\delta_0^*$ in the streamwise, wall-normal, and spanwise directions, respectively, where the reference boundary layer thickness δ_0 and displacement thickness δ_0^* are measured slightly upstream of the interaction region with the ramp. Both grids are composed by $N_x = 1440$, $N_r = 192$, and $N_\theta = 136$ points for a total of approximately 37.6 million points. The incoming perfect gas has a specific-heat ratio of $\gamma = 1.4$ and $T_\infty = 115K$. A quasi-adiabatic condition is considered by enforcing the total recovery temperature at the wall. The viscosity is calculated by Sutherland's law. Various particular probe locations are retained for the analysis, whose relative positions are illustrated in Fig. 2 (non-dimensionalized by the reference displacement thickness for a reference initial value corresponding to the domain inlet).

2 Simulation Results

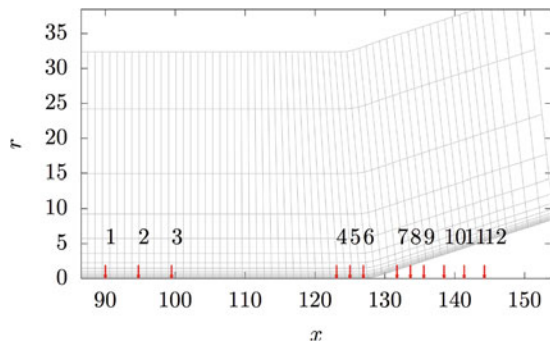
2.1 Upstream Boundary Layer Development

As expected, the transition mechanisms and subsequent development toward the fully turbulent state are not exactly similar in both cases. The final boundary layer characteristic thicknesses yet remain quite close. At the last observed position upstream of the interaction, the Reynolds numbers based on momentum thickness is however $Re_\theta = 1061$ for the flat case and $Re_\theta = 1161$ for the curved case. Some upstream wall-normal profiles of mean streamwise velocity and diagonal turbulent stress tensor components are shown in Fig. 3. They are extracted at the three first positions indicated in Fig. 2. They first confirm that the upstream distance is high enough to allow the development of a fully turbulent state. They also enhance some significant differences in the development of the turbulence structure. In particular, a significantly wider wake region is observed for the curved case by comparison with the flat case. The amplitude of the near-wall peak of turbulent stress is also slightly amplified for the curved case, more particularly for the streamwise and wall-normal stress components. The most significant difference between both cases is observed within the logarithmic region where the turbulent intensity is highly amplified for the curved case, and this increase of turbulent stress amplitude is more pronounced for the azimuthal component in the middle part of the boundary layer. This indicates a significant change of the anisotropy levels which might be associated with the shape alteration of the developing coherent structures while they move away from the wall.

2.2 Shock Wave-Boundary Layer Interaction

A snapshot of isosurfaces of Q criterion is illustrated for both cases in Fig. 4. It gives an overview of the topological differences observed in the shape and population density of near-wall coherent structures. The hairpin-like structures appear to be

Fig. 2 Mesh (zoom) in the interaction region (every 10 lines) and probe locations



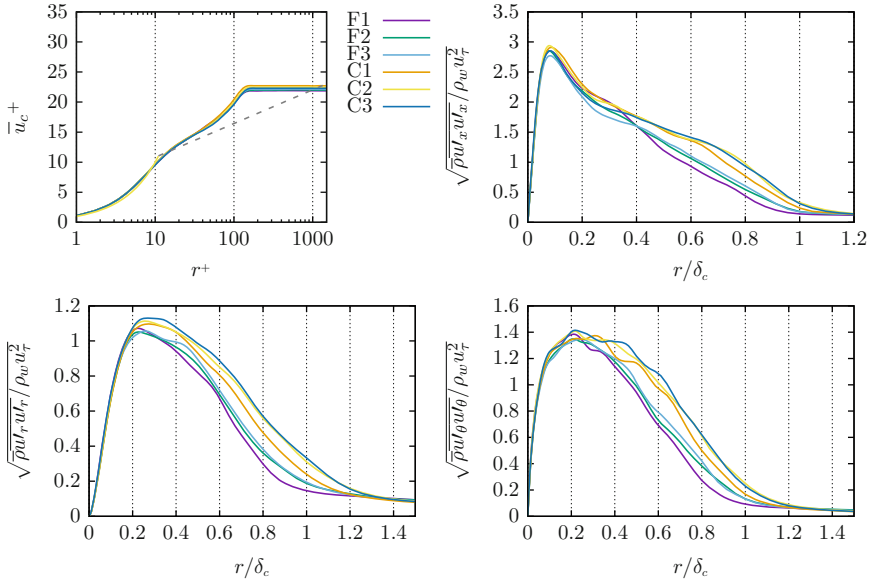


Fig. 3 Wall-normal profiles of streamwise velocity (van Driest transformed) (top left) and streamwise (top right), wall-normal (bottom left), and transverse (bottom right) turbulent stress components observed within the upstream developing supersonic boundary layer

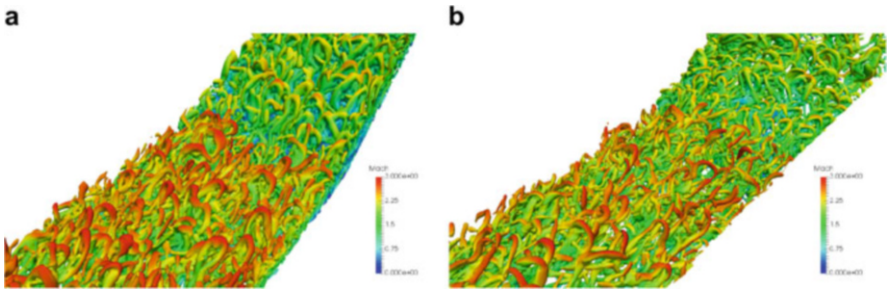


Fig. 4 Isosurface of Q criterion ($Q = 0.001 Q_{max}$) colored by values of Mach number. (a) Flat case. (b) Curved case

less numerous and more organized for the curved case in the upstream region and span through a larger area at the upper part of the boundary layer. This behavior might be expected from the presence of a larger flow section in the curved case available for the structures moving away from the wall. On the contrary, the passage through the interaction region leads to a more significant intensification of three-dimensional interactions for the curved case, while the largest structures at the upper part of the boundary layer appear more stretched in the streamwise direction for the flat case. Even if the pressure gradient and the extension of the subsequent separation region are significantly reduced in the curved case, it should be noted

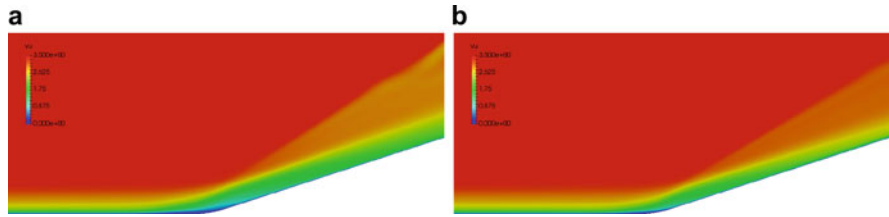


Fig. 5 Distribution of mean streamwise velocity in the interaction region. (a) Flat case. (b) Curved case

that this feature persists downstream of the interaction region where intermittent backflow regions could be observed. This limitation of the outward extension of the largest structures while increasing azimuthal motions and interactions thus seems to be mainly associated with the downstream transverse curvature present in the conical case.

In addition to this expected different pressure gradient between both cases, it is important to note also that the flow globally accelerates downstream of the interaction region in the conical case, whereas it tends toward a uniform state for the planar configuration. This naturally leads to a less important relative thickening of the boundary layer in the interaction zone. It also leads to a reduced growth rate and a modified shape factor evolution of the boundary layer downstream of the interaction for the conical case by comparison to the planar case. This behavior is illustrated in Fig. 5 with the (time and azimuthal) average of streamwise velocity component. The reduced extent of the low-velocity region close to the ramp corner illustrates the subsequent reduced length of the separation zone.

A closer look at the evolution of the turbulence structure in the interaction region is given in Fig. 6 with the evolution of wall-normal profiles of mean streamwise velocity component and diagonal turbulent stress components. The corresponding positions are indicated in Fig. 2. The large discrepancy between the plateau levels of average streamwise velocity reached for each curved or planar case through the interaction just reflects the different evolution of wall-shear stress and friction velocity u_τ used to non-dimensionalize these velocity profiles.

The passage through the interaction region leads in both cases to the expected formation of a secondary peak of streamwise turbulent stress away from the wall, around $r/\delta_c \simeq 0.4$, which dominates the primary near-wall peak observed in the upstream attached boundary layer. This behavior is expected and consistent with the global process of boundary layer deflection and thickening. Due to the reduced interaction strength (less important pressure gradient and separation extension) in the conical case, the relative amplification of these turbulent stress levels remains more important for the planar case than for the curved case. The magnitude of this peak then rapidly decreases when the boundary layer recovers a more natural attached behavior. The evolutions of the other turbulent stress components also reflect this distortion and subsequent relaxation process, with a more intense amplification of wall-normal turbulent stress closer to the wall (around $r/\delta_c \simeq 0.2$)

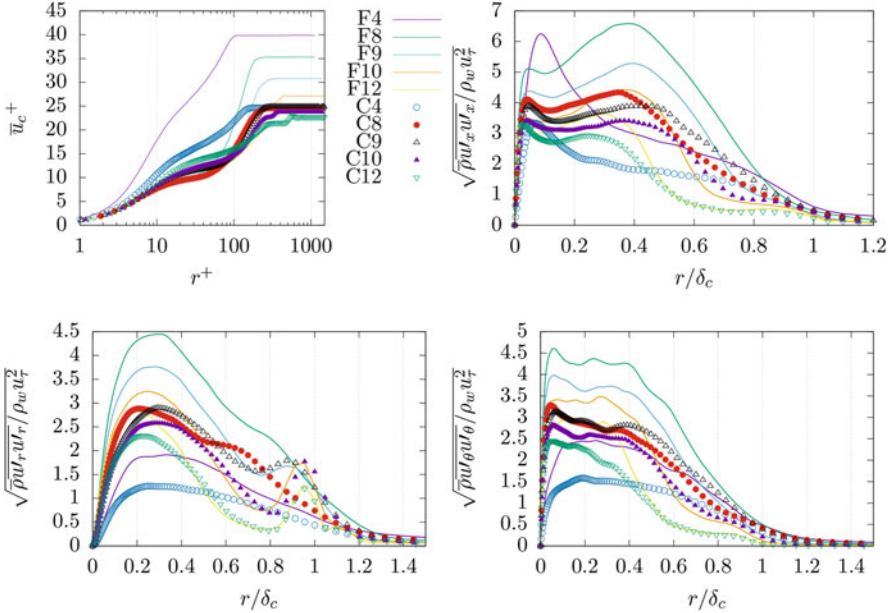


Fig. 6 Wall-normal profiles of streamwise velocity (van Driest transformed) (top left) and streamwise (top right), wall-normal (bottom left), and transverse (bottom right) turbulent stress components through the interaction region

and a topical formation of a wider range of intense transverse turbulent fluctuations (within the range $0.05 < r/\delta_c < 0.4$). Interestingly, the streamwise turbulent stress appears to relax quite similarly in both cases. However, the radial and transverse components behave differently between conical and planar cases. A secondary peak of radial turbulent stress is progressively formed close to the boundary layer edge in the conical case as we move in the downstream direction, which is not observed for planar configuration. In addition, the azimuthal turbulent stress component appears to relax far more slowly in the conical case than in the planar case. This behavior is consistent with the different azimuthal flow organization of turbulent flow structures in the downstream region, previously illustrated in Fig. 4. These results suggest that the increase of the available spatial extent in the azimuthal direction (when we move in the streamwise direction) allows to sustain transverse fluctuations generated through the interaction region.

3 Conclusion and Perspectives

Transverse curvature effects may be suspected to alter the properties of shock wave/boundary layer interactions. A preliminary assessment of these effects on the statistical turbulence structure of such an interaction has been given in the present

study through the analysis of direct numerical simulation data obtained in both supersonic planar ramp and conical/flare configurations. The expected decrease of shock intensity and subsequent interaction length in the conical case has been illustrated. The present results also suggest that the flow dynamics might be deeply altered with the emergence of new possible azimuthal modes organization. Further studies will be dedicated to the characterization of the dynamical features of such interactions.

Acknowledgements This work was performed using HPC resources from GENCI [IDRIS] (Grant i20172a7757).

References

1. M.F. Shahab, G. Lehnasch, T.B. Gatski, Streamwise relaxation of a shock perturbed turbulent boundary layer, in *Whither Turbulence and Big Data for the 21st Century*. Springer
2. N.T. Clemens, V. Narayanaswamy, Low-frequency unsteadiness of shock wave/turbulent boundary layer interactions. *Annu. Rev. Fluid Mech.* **46**, 469–492 (2014)
3. N.A. Adams, Direct numerical simulation of turbulent compression ramp flow. *Theor. Comput. Fluid Dyn.* **12**, 109–129 (1998)